

Synthesis of SO_4/ZrO_2 Catalyst and its Application in the Conversion of Ethanol to Diethyl Ether

Rena Septiyaningrum^a, Amalia Kurnia Amin^b, Wega Trisunaryanti^a, Karna Wijaya^{a,*}

a) Department of Chemistry, Faculty of Mathematics and Natural Sciences, Universitas Gadjah Mada, Yogyakarta 55281, Indonesia

b) Research Center for Chemistry, National Research and Innovation Agency, South Tangerang 15314, Indonesia

Received 13 July 2022; received in revised form 8 December 2022; accepted 24 December 2022 (DOI: 10.30495/IJC.2022.1963196.1948)

ABSTRACT

SO_4/ZrO_2 heterogeneous acid catalyst was prepared by wet impregnation method from ZrO_2 precursor involved variations in H_2SO_4 concentration (0.5; 1.0; 1.5 M) and calcination temperature (400, 500, 600 °C) to yield catalyst with the highest acidity value. The catalysts produced were characterized using Fourier Transform Infrared (FTIR) spectrometer, X-Ray Diffractometer (XRD), Scanning Electron Microscope-Energy Dispersive X-Ray (SEM-EDX), Thermogravimetry and Differential Scanning Calorimeter (TGA-DSC), Gas Sorption Analyzer (GSA), and acidity test using the gravimetric method with ammonia vapor. The catalyst used to observe activity and selectivity in the dehydration reaction of ethanol to diethyl ether (DEE) was SO_4/ZrO_2 catalyst with the highest total acidity. The liquid product from the dehydration of ethanol was analyzed using Gas Chromatography (GC). The ZS-1.5-500 catalyst showed the best activity and selectivity in the dehydration reaction of ethanol to DEE at a temperature of 225 °C, yielding 49.85% (w/w) ethanol conversion and a 1.62% DEE selectivity.

Keywords: Ethanol dehydration, Diethyl ether, Optimization, Catalysts, Sulfated zirconia

1. Introduction

The relentless use of fossil fuel, with it, the emission of gases that pollute the air, has contributed greatly to many environmental problems. To alleviate this effect, biofuels are being developed, with great potential, to replace petroleum-based energy sources. Biofuel created from biomass can help reduce dependence on oil imports and, ultimately, environmental problems as well [1]. Biofuels provide the advantages of being biodegradable, non-toxic, and able to reduce the emission of toxic gases and carbon dioxide from fossil fuel combustion processes in engines [2]. Among these biofuels, bioethanol has attracted many interests as it offers good combustion efficiency attributable to its high octane content and favorable energy density [1]. It also offers reduced combustion temperature in an engine that would lower emissions of sulfur oxides (SO_x) and nitrogen oxides (NO_x) [3–5]. Unfortunately, ethanol is

difficult to separate or make pure water as the two forms of an azeotropic mixture at a temperature of 78.15 °C with an azeotropic point of 95.57% [6]. To remedy this complication, ethanol can be converted to diethyl ether (DEE). Diethyl ether has shown promising potential as a substitute for fossil fuels as it exhibits good activity even in cold weather due to its high volatility and low flash point [7]. Diethyl ether as a mixture is able to increase combustion due to the high octane number (> 100), cetane number (> 125), and oxygen content, all favoring its role as an additive to diesel or biodiesel [8].

Diethyl ether can be produced from the dehydration process of ethanol using an acid catalyst such as H_2SO_4 (Barbet process) [7]. However, such a conventional approach in using homogenous acid catalysts, though producing high yields, poses the disadvantages of potential corrosion and poor separation of the catalyst from the product [9,10]. In its stead, heterogeneous catalysts can be used to circumvent these disadvantages. Correspondingly, studies have been carried out on the

*Corresponding author:

E-mail address: karnawijaya@ugm.ac.id

(K. Wijaya)

use of solid acid catalysts such as metal-doped zeolite [10,11], modified montmorillonite [12], phosphated and metal-doped alumina [9,13,14], metal-sulfated and sulfated titania [15,16], hydrotalcite-like compound (HTC) [17,18], and heteropoly acids (HPA) [19] in the dehydration process of ethanol to DEE. Generally, product yield selectivity depends on the nature of the acidic site and type, and also reaction conditions, especially temperature [17,19]. Brønsted acid sites play an important role in the ethanol to DEE dehydration over heteropoly acid catalysts [19]. In modified alumina and HTC catalysts, a high Al–OH surface concentration enhances the dehydration path increasing DEE yield [17]. Higher Lewis acid sites than Brønsted acid sites lead to a greater degree of DEE cracking reaction, resulting in a decrease in DEE selectivity and an increase in ethylene selectivity [9].

Zirconium dioxide (ZrO_2) is a metal oxide that can act as a catalyst [20,21]. The surface of ZrO_2 contains both acidic and basic sites that can be used in the synergistic reactions of acid-base catalysts such as alcohol dehydration, carbon dioxide activation, and formic acid decomposition [22–25]. However, the reactivity of ZrO_2 in alcohol dehydration reaction is very low [26]. According to [10], the acid strength of a catalyst, associated with its Brønsted and Lewis acid sites, greatly affects the catalytic activity of the catalyst in the dehydration reaction of ethanol. The role of Brønsted and Lewis acids in the catalyst can be bolstered by the addition of, among other things, sulfate (SO_4^{2-}) [27]. As such, sulfate ion-modified zirconia has higher acidity than just ZrO_2 as the presence of the two acid sites, namely the Lewis acid site and Brønsted acid site, are made more prominent with the modification [28]. SO_4/ZrO_2 catalyst has been reported to be successfully applied in several catalytic reactions [29–31]. Based on this, SO_4/ZrO_2 catalyst synthesized from ZrO_2 precursor and H_2SO_4 through the wet impregnation method is expected to have catalytic ability attributable to the presence of Lewis acid and Brønsted acid sites. Moreover, the catalyst would have great potential to be applied in the dehydration reaction of ethanol to DEE. The combination of ZrO_2 precursor and H_2SO_4 is expected to offer a relatively shorter catalytic reaction time because it would not produce cations and anions impurities and minimize the waste generated.

2. Experimental

2.1. Materials

Commercial zirconium dioxide (ZrO_2) was bought from Hongwu International Group Ltd, China. Pro analysis chemicals namely, sulfuric acid (H_2SO_4 98%), ethanol

(C_2H_5OH 96%), and ammonia (NH_3) were produced from Merck, Germany, while nitrogen gas (N_2) was supplied from Samator Gas Ltd., Indonesia.

2.2. Catalyst preparation

Sulfated zirconia (SO_4/ZrO_2) catalysts were prepared by wet impregnation method according to our previous method, with modification [32]. Typically, 10.0 g of commercial ZrO_2 was reacted with a 150 mL solution of H_2SO_4 (0.5, 1.0, and 1.5 M) and stirred continuously for 24 hours at room temperature. The resulting mixtures were then centrifuged at 2000 rpm for 20 min. The obtained solids were dried at 105 °C for 24 hours and were denoted as ZS-0.5, ZS-1.0, and ZS-1.5. The samples were then characterized using FTIR and NH_3 adsorption for acidity tests. The as prepared SO_4/ZrO_2 with the highest acidity was calcined at temperatures of 400, 500, and 600 °C for 4 hours and denoted as ZS-1.5-400, ZS-1.5-500, and ZS-1.5-600. Those samples were tested for acidity again to distinguish the highest total acidity.

2.3. Catalyst Characterization

Catalysts were characterized using a Fourier Transform Infrared spectrometer (FTIR, Shimadzu IR Prestige 21, Japan) to study their functional groups. X-Ray Diffraction (XRD, X'pert Pro PANalytical, Germany) was used to determine the crystallinity, crystalline phase, and crystal size of the catalyst. Characterization using Scanning Electron Microscope - Energy Dispersive X-Ray (SEM-EDX, Hitachi SU3500, Japan) was performed to determine the surface characteristics and elemental composition of the sample. The thermal stability and degradation phenomena of components in the sample based on enthalpy changes were characterized by Thermal Gravimetric Analyzer and Differential Scanning Calorimeter (TGA-DSC, Linseis TA PT 1600, Germany). Gas Sorption Analysis (GSA, Quantachrome NOVA, USA) touch was aimed to measure the surface area and pore size of the catalyst. The total acidity of catalysts was quantitatively analyzed through an acidity test using the gravimetric method (equation 1) with ammonia vapor as an adsorbate base (mmol sorbed NH_3 per gram sample). The empty porcelain crucible was heated at 100 °C for 1 hour, then weighed as W_0 . A 0.05 g of the catalyst sample was put into an empty porcelain crucible, heated for 1 hour at 100 °C, and then weighed as W_1 . The crucible containing the sample was placed in a closed desiccator filled with ammonia vapor and the sample was allowed to stand for 24 hours, weighed as W_2 .

$$\text{Total acidity} = \frac{W_2 - W_1}{(W_1 - W_0) \times M_r NH_3} \times 1000 \quad (1)$$

2.4. Activity Test of Catalytic and Product Analysis

ZrO₂ and ZS-1.5-500 catalysts were used in the dehydration process of ethanol to diethyl ether (DEE). The conversion process of ethanol into DEE was carried out in a fixed-bed reactor (**Fig. 1**) under atmospheric pressure which was fed with N₂ as a carrier gas at a flow rate of 20 mL/minute with a temperature variation of 175, 200, and 225 °C for 2 hours using 0.4 g of catalyst and 10 mL of ethanol. The converted liquid product was analyzed using Gas Chromatography with a flame ionization detector (GC-FID, Agilent Hewlett Packard HP 5890 Series II, USA). The liquid product ethanol conversion (X_{EtOH}) and product selectivity or DEE content (S_{DEE}) were calculated from the result of chemical composition using equations (2) and (3). Where m_{EtOH} , E_{DEE} , and E_{total} are the mass of ethanol, the peak area of DEE from gas chromatogram, and the total peak area from gas chromatogram, respectively.

$$X_{\text{EtOH}}(\%) = \frac{m_{\text{EtOH}}(\text{in}) - m_{\text{EtOH}}(\text{out})}{m_{\text{EtOH}}(\text{out})} \times 100\% \quad (2)$$

$$S_{\text{DEE}}(\%) = \frac{E_{\text{DEE}}}{E_{\text{total}}} \times 100\% \quad (3)$$

3. Results and Discussion

3.1. Characterization of catalysts

3.1.1. FTIR and acidity test

Fig. 2 shows FTIR spectra of ZrO₂ and SO₄/ZrO₂ of various sulfate concentrations. The spectra showed a wide absorption band in the wavenumber region of

3400–3500 cm⁻¹ denoting the stretching vibration of the O–H bond and a sharp band at 1635 cm⁻¹ denoting the bending vibration of the O–H bond in the H₂O molecule [27,33,34]. The intensity of the absorption band of the O–H group and water molecules appeared to increase along with the increase in the concentration of SO₄²⁻ used in the sulfation process. The presence of new bands that appeared in the wavenumber range of 956–1474 cm⁻¹ in ZS-0.5, ZS-1.0, and ZS-1.5 confirmed the success of catalyst activation with SO₄²⁻ indicated by the characteristic band of a bidentate chelate of SO₄²⁻ covalently coordinated to Zr⁴⁺ cation commonly observed in this spectral region [35]. The new absorption bands that appeared at wavenumbers 956–1003, 1057–1096, 1157, and 1226 cm⁻¹ denoted the S–O symmetric vibration, S–O asymmetric vibration, S=O symmetric vibration, and S=O asymmetric vibration, respectively [36]. This is suggested that the acidity of Zr⁴⁺ cation as a Lewis acidic site for ZS-0.5, ZS-1.0, and ZS-1.5 were stronger than pure zirconia. The acidic strength of Zr⁴⁺ ions increased by the inductive effect of S=O from SO₄²⁻, while the presence of Brønsted acidic sites are proved by the appearance of S=O band [32,37–39]. The intensities of absorption bands typical to the sulfate ions continued to increase from ZS-0.5 to ZS-1.5, which can be an early indication of an increase in acidic strength as the concentration of sulfuric acid used increases. The four spectra of pure zirconia and the modified samples all presented absorptions in the wavenumber range of 501–740 cm⁻¹ which represented the Zr–O–Zr stretching vibration [23,40].

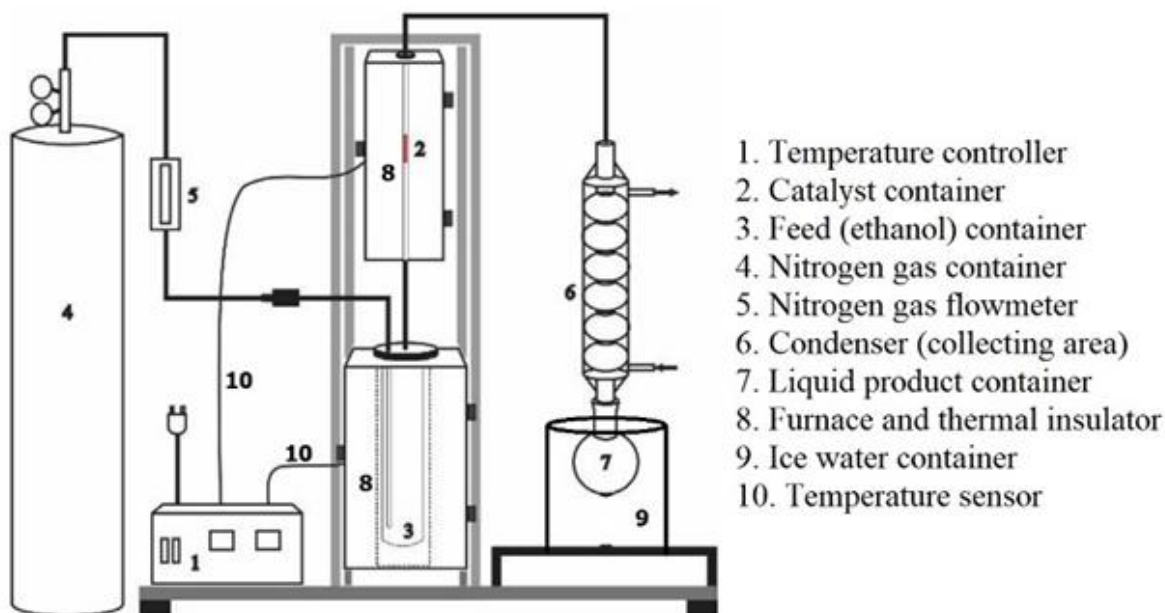


Fig. 1. The schematic diagram of the dehydration reactor

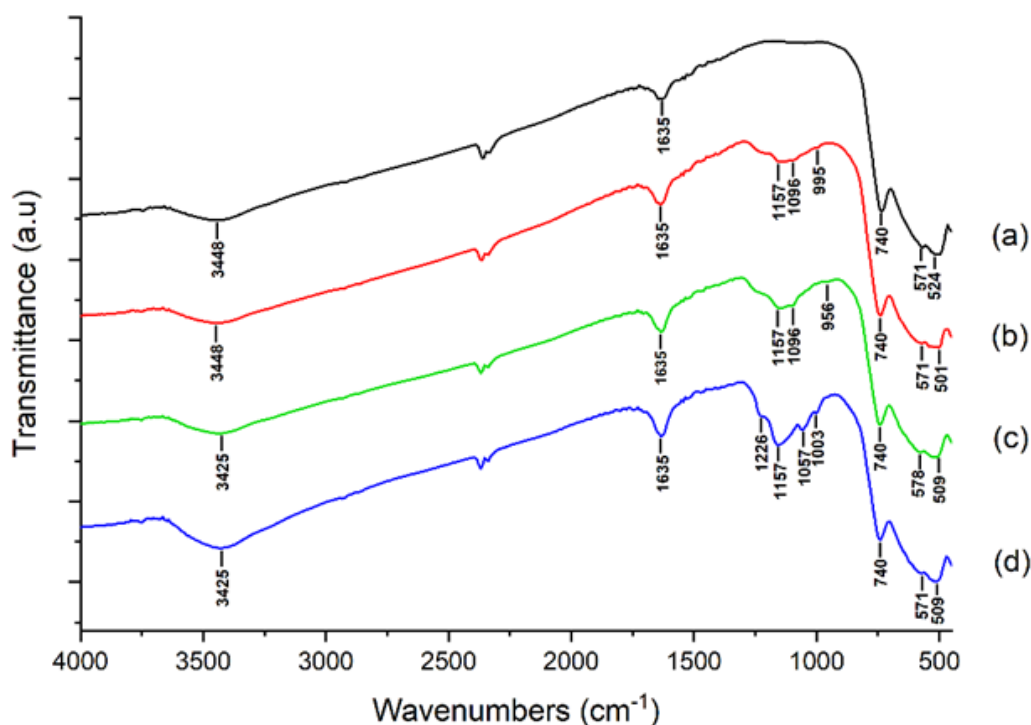


Fig. 2. FTIR spectra of (a) ZrO_2 (b) ZS-0.5 (c) ZS-1.0 (d) ZS-1.5

Table 1 shows the total acidity of the catalyst at various concentrations obtained through the acid test using the gravimetric method. Total acidity is the number of Brønsted acid and Lewis acid sites within a material calculated based on the ability of the catalyst to adsorb ammonia gas. **Table 1** shows that pure ZrO_2 had a very low total acidity, which was $0.348 \text{ mmol g}^{-1}$. The acidity of the zirconia material originated from the Zr^{4+} cations that act as Lewis acid sites. From ZS-0.5 to ZS-1.0 and then ZS-1.5, total acidity was observed to increase with the highest total acidity, as obtained by ZS-1.5, of $1.984 \text{ mmol g}^{-1}$. The higher concentration of sulfuric acid used in the sulfation process has increased the acidity of the catalyst as the number of ions on the zirconia surface increased and made optimal the adsorption of ammonia [41].

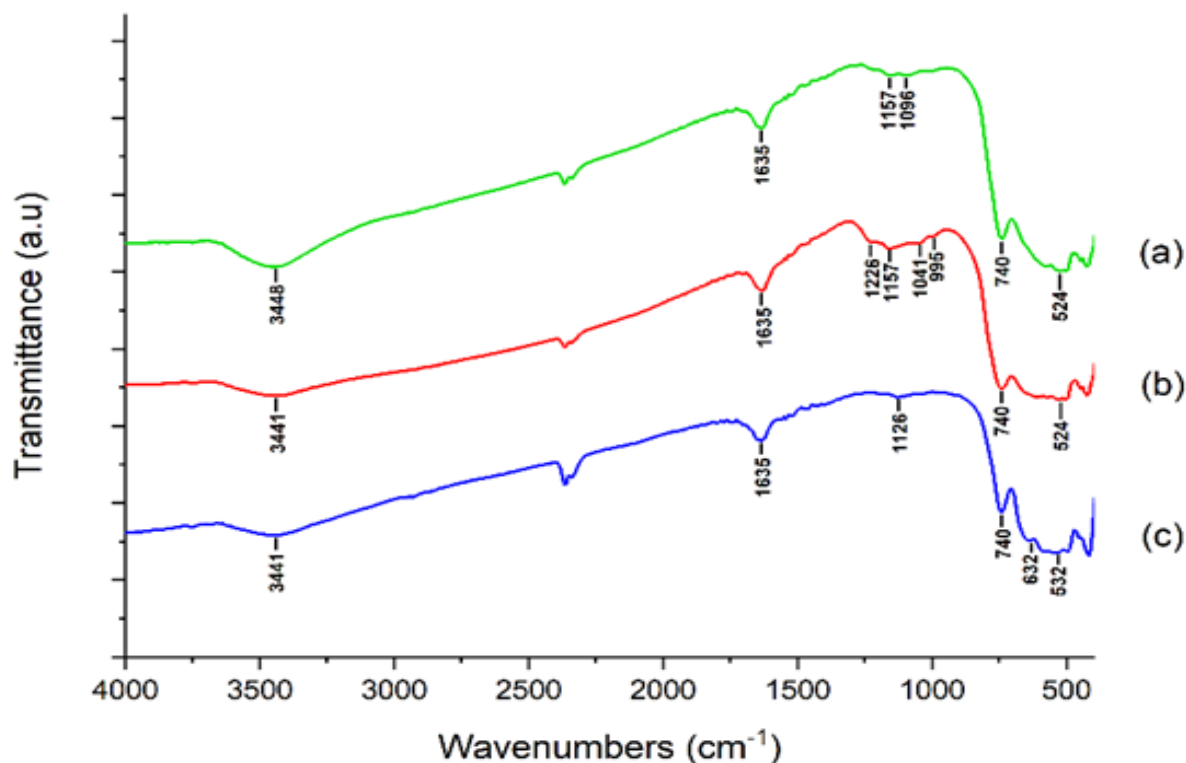
Changes to the sulfate ion absorption bands due to the influence of calcination temperatures are shown in **Fig. 3**. The sulfate ion absorption band had the greatest intensity at the calcination temperature of $500 \text{ }^\circ\text{C}$ and decreased when it reached $600 \text{ }^\circ\text{C}$. This indicated that the temperature of $500 \text{ }^\circ\text{C}$ was the optimum calcination temperature for the $1.5 \text{ M SO}_4/\text{ZrO}_2$ catalyst, whereby at the temperature of $600 \text{ }^\circ\text{C}$, the catalyst underwent sulfate ion decomposition indicated by the disappearance of the sulfate ion absorption bands. The effect of calcination temperature on the acidity of ZS-

1.5-400, ZS-1.5-500, and ZS-1.5-600 catalysts can be observed in **Table 2**. The total acidity increased from the temperature of $400 \text{ }^\circ\text{C}$ to $500 \text{ }^\circ\text{C}$, namely from $1.342 \text{ mmol g}^{-1}$ to $2.392 \text{ mmol g}^{-1}$. This value decreased at the calcination temperature of $600 \text{ }^\circ\text{C}$ to $1.742 \text{ mmol g}^{-1}$. That is, high calcination temperatures can cause a decrease in the number of acid sites on the catalyst [42].

Fig. 4 compares the spectra of ZrO_2 and ZS-1.5-500 materials after the adsorption of ammonia vapor. The FTIR spectra of sorbed ammonia on ZrO_2 and SO_4/ZrO_2 were obtained in distinguishing among Brønsted and Lewis acidic sites as well as estimating estimate their amounts. At $1111\text{--}1118 \text{ cm}^{-1}$ an absorption band appeared in both ZrO_2 and ZS-1.5-500 catalysts. According to [43,44], this band denoted the vibration of ammonia (NH_3) coordinated to the Lewis acid site (Zr^{4+}) of the catalyst material. At the wavenumber of 1404 cm^{-1} , ZS-1.5-500 showed a new absorption band, indicating the vibration of ammonium ion (NH_4^+) formed due to proton transfer from Brønsted acid site (OH group) to NH_3 . Within the commercial ZrO_2 , the intensity of the Lewis acid site absorption band was very low and the Brønsted acid site was almost undetectable. In contrast, the SO_4/ZrO_2 catalyst had a relatively higher intensity of absorptions for the Lewis and Brønsted acid sites. The structural properties and surface acidities of the catalysts strongly influenced the catalytic activity [45].

Table 1. Catalyst acidity test

Catalyst	Total Acidity (mmol g ⁻¹)
ZrO ₂	0.348
ZS-0.5	1.245
ZS-1.0	1.520
ZS-1.5	1.984

**Fig. 3.** FTIR spectra of (a) ZS-1.5-400 (b) ZS-1.5-500 (c) ZS-1.5-600**Table 2.** Total acidity of ZS-1.5 400, 500, and 600 °C

Catalyst	Total Acidity (mmol g ⁻¹)
ZS-1.5-400	1.342
ZS-1.5-500	2.392
ZS-1.5-600	1.742

3.1.2. XRD characterization

Fig. 5 presents the XRD pattern of ZrO₂ and ZS-1.5-500 recorded at $2\theta = 4-80^\circ$. XRD analysis presented that the two catalysts had prominent diffraction peaks at around $2\theta = 28^\circ, 31^\circ,$ and 50° with hkl values (-110), (111), and (220). According to JCPDS No. 86-1449, these three diffraction peaks referred to the monoclinic phase of ZrO₂. The two XRD patterns all confirmed the sole presence of the monoclinic crystal phase. The crystalline phase structure showed stability after sulfation and calcination treatment. However, the ZS-1.5-500 catalyst which was the catalyst made from zirconia modified with 1.5 M sulfuric acid and calcined

at 500 °C had lower intensity diffraction peaks compared to untreated ZrO₂. Precisely at the monoclinic peaks $2\theta = 28^\circ$ and 31° their intensities changed. This indicated that the sulfation and calcination steps had influenced the degree of crystallinity of the catalyst. According to [23], sulfate groups added would blanket the surface of ZrO₂, thereby inhibiting crystal growth and intensities observed. Research by [23] on the synthesis of sulfated zirconia using ZrO₂ precursor calcined at a temperature of 600 °C produced a sulfated zirconia catalyst with a monoclinic crystalline phase structure. The average crystal size (D) of each catalyst (pure and modified) was calculated based on the Debye-Scherrer equation, $D = K\lambda/\beta\cos\theta$. Modification with sulfuric acid on ZrO₂

resulted in increased crystal size of the constituent material. Based on the calculations, the average crystal size of ZrO_2 was 29.15 nm, increasing to 31.03 nm with modification using sulfate. In accordance with [35,36,45], sulfate incorporation lowered the peak

intensities and increased the crystallite size. It may imply a decrease in Zr–Zr coordination and an increase in structural disorder due to sulfate species. Calcination temperature may also lead to crystallite growth due to loss of H_2O .

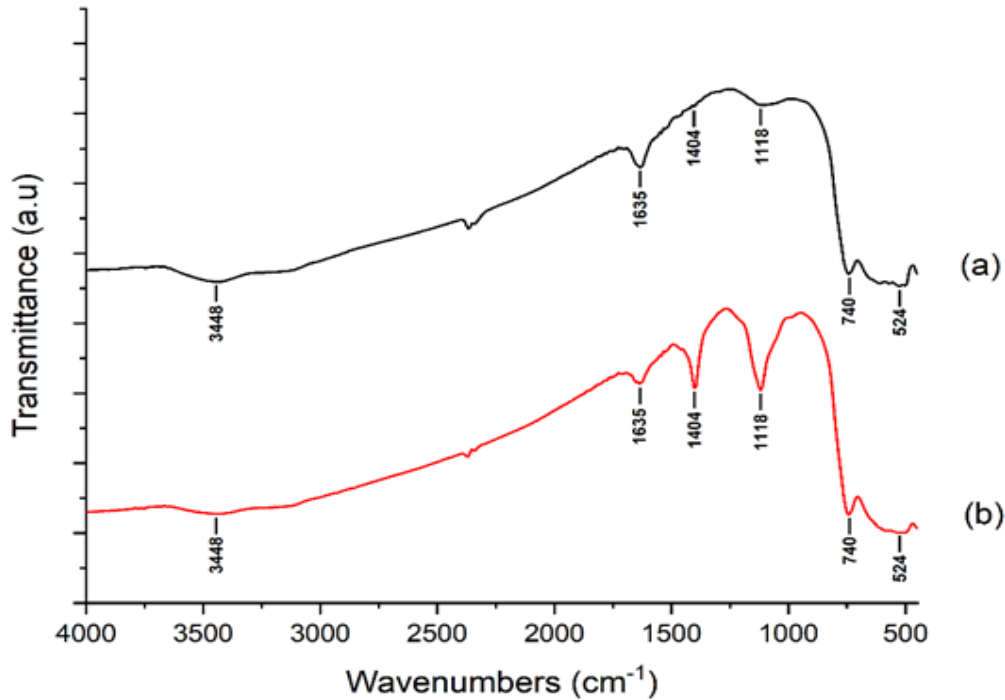


Fig. 4. FTIR spectra of (a) ZrO_2 (b) ZS-1.5-500 after acidity analysis

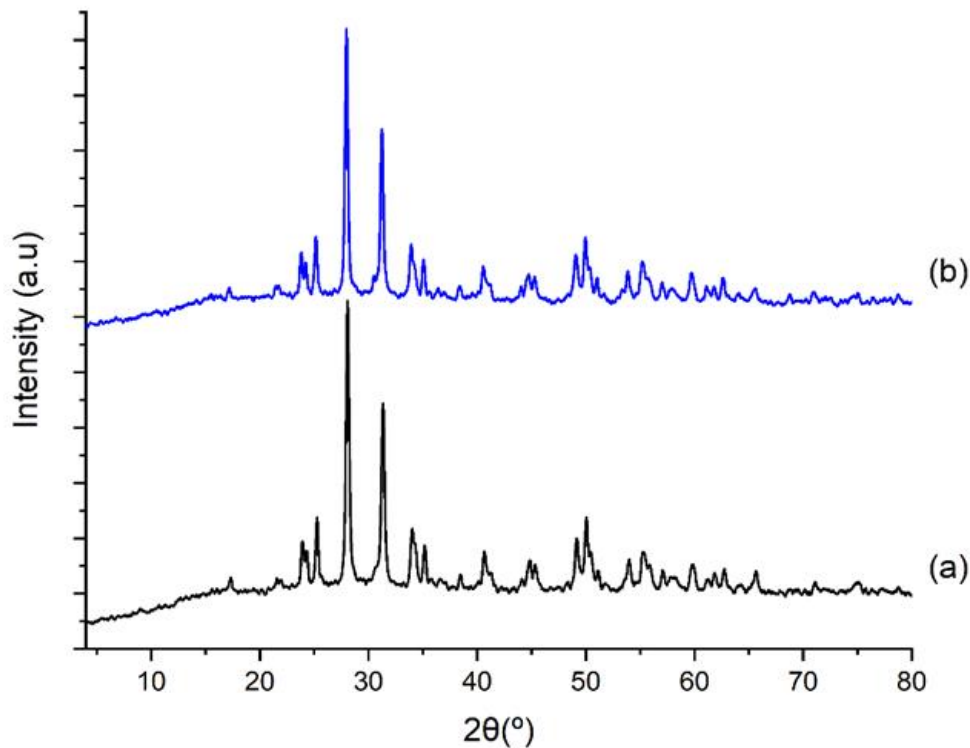


Fig. 5. XRD pattern of (a) ZrO_2 (b) ZS-1.5-500

3.1.3. SEM-EDX characterization

Fig. 6 shows the surface morphologies of unmodified and sulfate-modified zirconia catalysts captured using SEM. Both morphologies presented rough surface structures and irregular shapes. The surface morphology of the sulfated and calcined zirconia (SO_4/ZrO_2) showed the formation of agglomeration of particles into granules more frequently than that of the commercial ZrO_2 material. The ZS-1.5-500 catalyst also showed a larger and non-uniform size. This was due to the incorporation of small crystallites during the calcination process [46]. Incidentally, the success of the sulfate ion attachment process on the surface of the catalyst can be identified using EDX by referring to the presence of O and S elements. Data of the mass percentage of elements are shown in **Table 3**, whereby ZS-1.5-500 had a mass percentage of sulfur of 0.6%. This indicated that sulfate ions have been successfully deposited on the surface of ZrO_2 .

3.1.4. TGA-DSC characterization

The TGA curve of ZrO_2 , shown in **Fig. 7a**, had a relatively linear horizontal shape and did not demonstrate a significant decrease in mass at 30–900 °C thermal treatment. This suggested that the ZrO_2 material used had good thermal stability. In the temperature range of 50–220 °C, there was a decrease in mass of 2.00% attributable to the elimination of water molecules adsorbed on the sample. Based on the DSC curve, in this temperature range, there was an endothermic occurrence due to the release of water molecules.

The TGA curve of the ZS-1.5-500 catalyst treated to a temperature of 900 °C is shown in **Fig. 7b**. The decrease in mass of 1.358% occurred at a temperature range of 50–200 °C and could be associated with the loss of water molecules adsorbed on the catalyst material. The decrease in mass in this temperature range was accompanied by the formation of an absorption peak on the DSC curve which indicated an endothermic reaction from the process of releasing water molecules. In the temperature range of 530–700 °C, a decrease in mass of 5.864% was also identified. This phenomenon indicated the decomposition of sulfate ions bound to the catalyst [34,45].

3.1.5. Surface area analysis

The surface area of the catalyst decreased from 11.112 $\text{m}^2 \text{g}^{-1}$ (ZrO_2) to 9.738 $\text{m}^2 \text{g}^{-1}$ (ZS-1.5-500) after sulfation and calcination. A similar decrease was also shown by the pore volume data, with the pore volume of ZrO_2 of 0.051 $\text{cm}^3 \text{g}^{-1}$ decreased to 0.040 $\text{cm}^3 \text{g}^{-1}$ after

Table 3. Elemental compositions of ZrO_2 and ZS-1.5-500

Catalyst	Mass (%)		
	Zr	O	S
ZrO_2	58.7	41.3	-
ZS-1.5-500	55.1	44.3	0.6

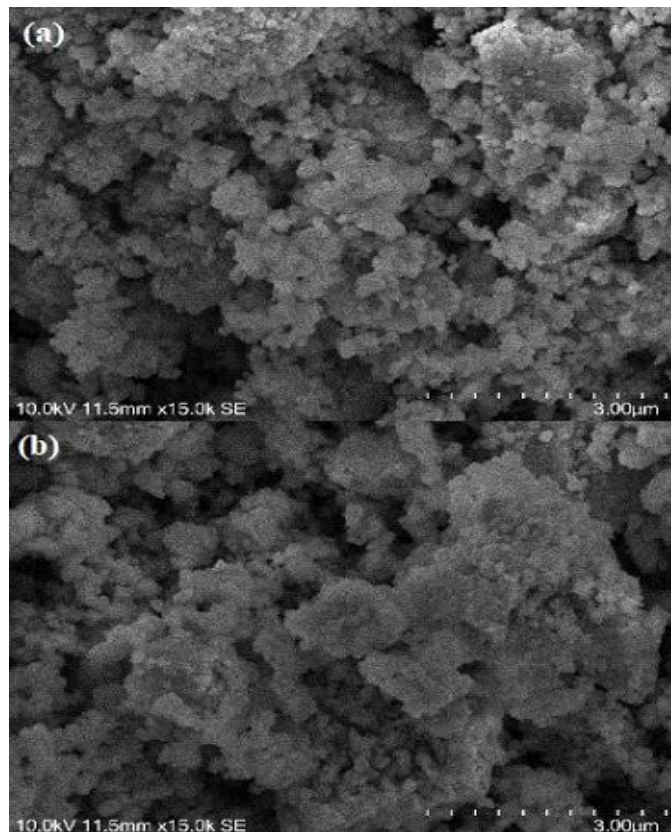


Fig. 6. SEM images of (a) ZrO_2 (b) ZS-1.5-500

treatments (**Table 4**). The decrease in specific surface area and total pore volume in the ZS-1.5-500 catalyst indicated that the sulfation treatment caused the surface pores of the zirconia to be covered by sulfate ions [41]. This data is in line with the XRD results that implied that the addition of sulfate ions to ZrO_2 had reduced the intensity of the main diffraction peak of the ZrO_2 monoclinic crystalline phase.

The average pore diameters for ZrO_2 and ZS-1.5-500 samples were 18.277 nm and 16.354 nm, placing both in the mesoporous material category (**Table 4**). Research by [47] reported that the synthesis of SO_4/ZrO_2 using the impregnation method with calcination treatment at a temperature of 500 °C obtained an average pore diameter of 15.8 nm, and thus was a mesoporous material. The isotherm curves from the N_2 gas adsorption and desorption of the two catalysts are shown in **Fig. 8**. According to the IUPAC classification, the two curves follow the type IV isotherm pattern typical

of mesoporous materials. According to [48], materials of this type demonstrate monolayer adsorption followed by multilayer formation due to capillary condensation. The presence of hysteresis loops in the multilayer region

is a characteristic of mesoporous materials that occurs due to capillary condensation at different relative pressures. Both catalysts exhibited H3-type hysteresis.

Table 4. Textural characteristics of ZrO₂ and ZS-1.5-500

Catalyst	Specific surface area (m ² g ⁻¹)	Total pore volume (cm ³ g ⁻¹)	Average pore diameter (nm)
ZrO ₂	11.112	0.051	18.277
ZS-1.5-500	9.738	0.040	16.354

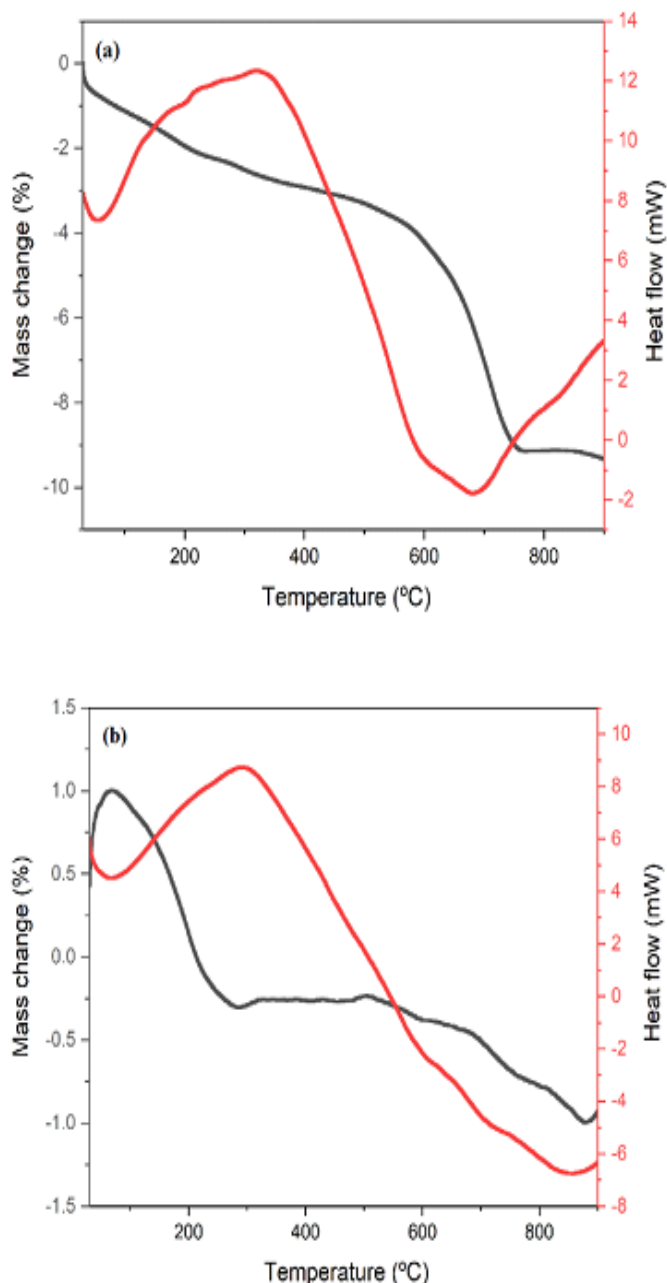


Fig. 7. TGA/DSC curves of (a) ZrO₂ (b) ZS-1.5-500

3.2. Catalyst application

3.2.1. Catalytic activity towards dehydrated liquid product

In order to determine the catalytic ability of SO₄/ZrO₂ to convert ethanol into liquid products, in particular, diethyl ether (DEE), a catalytic activity test was carried out in the temperature range of 175–225 °C. The ethanol dehydration process was carried out for 60 minutes with an N₂ gas flow at a rate of 20 mL/minute. The ethanol dehydration process produced 3 types of products, which were non-condensable gas products, liquid products, and residues. The catalytic activity of this experiment was focused on obtaining the resulting liquid products.

The percentage of ethanol conversions gained from the dehydration reaction using the two catalysts is presented in **Fig. 9**. The data presented compares the yield of liquid products from the use of ZrO₂ and ZS-1.5-500 catalysts at reaction temperatures of 175, 200, and 225 °C. The increase in the temperature of the reaction was accompanied by an increased in the conversion of ethanol in both, with conversions at 175, 200, and 225 °C of 22.06%, 26.47%, and 29.85% for ZrO₂ catalyst, and 35.45%, 41.82%, and 49.85% for ZS-1.5-500 catalyst. Autthanit and Jongsomjit [11] reported similar results, where the ethanol conversion increased with increasing reaction temperature in the ethanol dehydration reaction. However, the ZS-1.5-500 catalyst resulted in higher ethanol conversion yields than the ZrO₂ catalyst at all temperatures. This implies the existence of sulfate ions on the surface of ZrO₂ enhances the total acidity of the catalyst by increasing the number of Brønsted and Lewis acid sites. This result in good agreement with [16,45] which sulfate surface essentially influences improving catalytic activity. The dehydration of alcohols is acid-catalyzed [7,45], so even though both

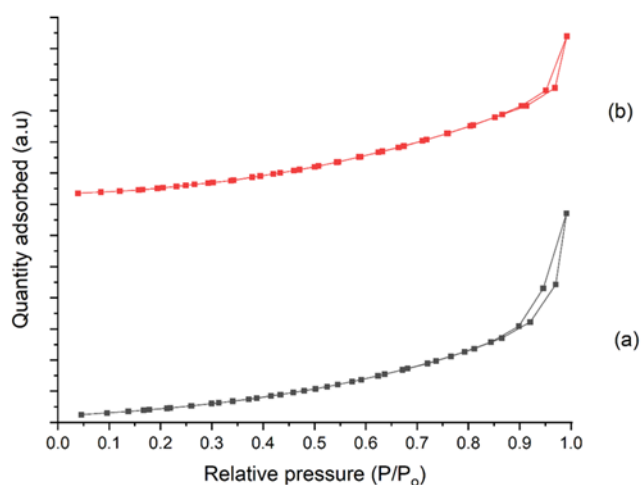


Fig. 8. Adsorption-desorption isotherm curves of (a) ZrO_2 and (b) ZS-1.5-500

ZrO_2 and ZS-1.5-500 catalyst has a low surface area, the yield is still high as those acidic properties are taking control. According to [10,19,45], the acid strength of a catalyst's Brønsted and Lewis acid sites has a significant effect on the catalytic activity of the catalyst in the ethanol dehydration reaction.

3.2.2. Catalyst selectivity towards dehydrated liquid products

The DEE selectivity of the ZrO_2 catalyst was compared to that of ZS-1.5-500, a sulfate-modified commercial ZrO_2 with the highest acidity level. The results can be seen in **Fig. 10**. The spiking method determined the amount of DEE in the liquid product conversion (yield).

The sample (each yield) is analyzed using Gas Chromatography (GC) after a standard DEE compound has been added. Compound analysis was carried out by comparing the intensity of the peaks before and after spiking. If the same component is introduced to the standard compound and the compound being examined, the intensity will increase.

Based on **Fig. 10**, ZrO_2 and ZS-1.5-500 catalysts showed significant differences in selectivity toward DEE. Dehydration reaction using the ZrO_2 catalyst produced liquid products with no diethyl ether content, i.e., 0% DEE, at all temperature variations. However, the catalytic reaction involving the ZS-1.5-500 catalyst indicated the presence of DEE in the resulting product. There was an increase in DEE levels from 0.64%, 1.33%, and 1.62% as temperature increased from 175, 200, and then 225 °C. The difference in these results indicated that the reaction temperature played a major role in determining the dehydration reaction of ethanol to DEE. Thus, it can be concluded that the optimum condition for the ZS-1.5-500 catalyst in the dehydration reaction of ethanol to diethyl ether is at the temperature of 225 °C. The significant difference in the DEE content between the ZrO_2 and ZS-1.5-500 catalysts was due to the different acid properties of the two catalysts, whereby the ZrO_2 material only had low strength Lewis acid sites and minimum Brønsted sites on the surface. On the other hand, the ZS-1.5-500 catalyst had a higher amount of Brønsted and Lewis acid sites due to the presence of sulfate ions on the ZrO_2 surface, thereby increasing the acidity and selectivity of the catalyst.

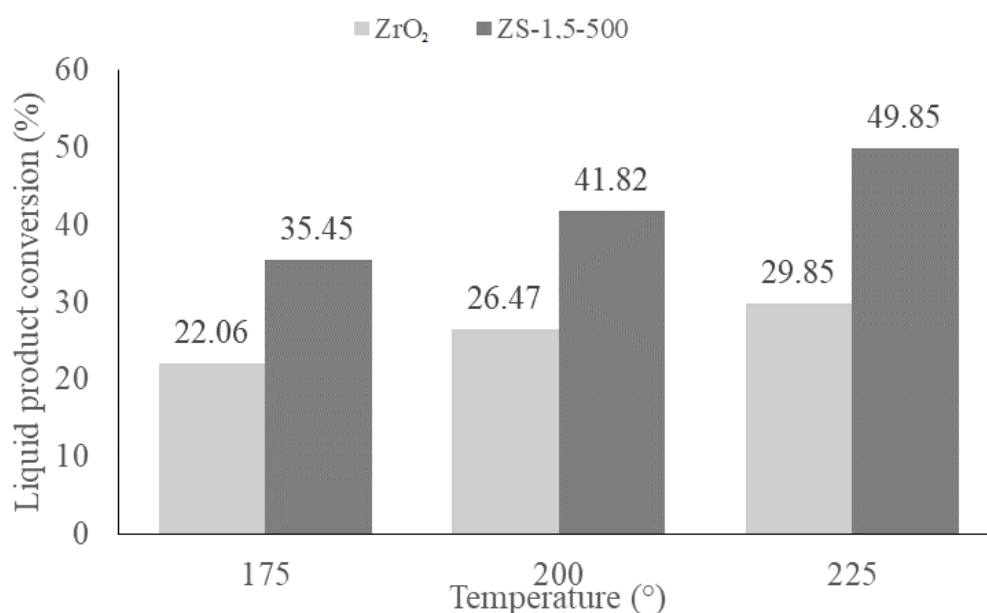


Fig. 9. Liquid product conversion from the dehydration reaction

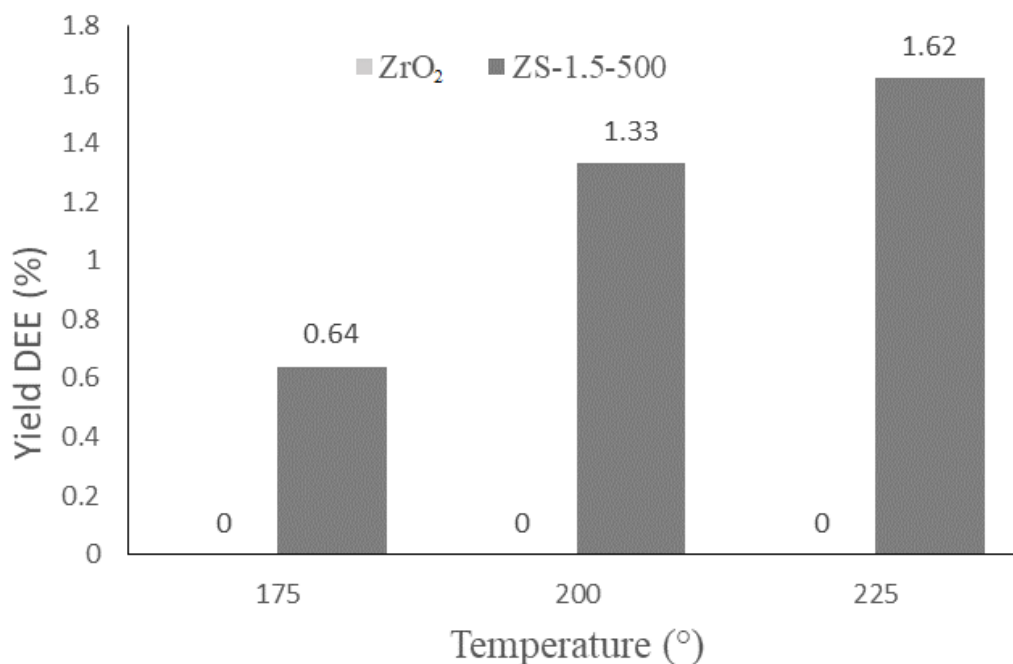


Fig. 10. DEE content at the different dehydration reaction temperatures

Research by Kamsuwan et al. [49] reported the use of heterogeneous alumina catalysts in the dehydration reaction of ethanol to produce DEE with levels reaching 3% at 200 °C and 12% at 250 °C. Yet, the use of an SO₄/ZrO₂ catalyst resulted in higher DEE levels than the use of a phosphate-modified alumina catalyst. Limlamthong et al. [13] studied the effect of phosphoric acid addition to alumina catalyst on the dehydration process of ethanol to DEE. The use of catalysts at temperatures of 200 and 225 °C did not produce DEE. Thus, the dehydration process of ethanol into DEE using heterogeneous catalysts still showed relatively lower yields than using homogeneous catalysts, such as H₂SO₄ in the Barbet process.

The pore size of the catalyst can also affect the yield of the DEE product. Research related to the conversion of ethanol to DEE has also been carried out by Marbun et al. [50] using an alumina catalyst with a Cr-Co promoter with the highest DEE content obtained at 0.3%. This catalyst had a pore diameter of 0.23 nm, smaller than the SO₄/ZrO₂ catalyst with a pore diameter of 16.354 m² g⁻¹. The pore diameter of the SO₄/ZrO₂ catalyst was more appropriate for the molecular size of diethyl ether (0.667 nm), meaning that the dehydration reaction could run better and produce higher DEE levels.

4. Conclusions

A Series of sulfated zirconia was successfully prepared from commercial ZrO₂, and its incorporation impacted on increasing exposed Brønsted and Lewis acidic active sites on its surface. The optimum calcination condition of sulfation was 500 °C. The SO₄/ZrO₂ surface consists of higher exposed acidic sites on mesoporous aggregate nanocrystals. Its character was able to increase the activity and selectivity of the catalyst in the diethyl ether (DEE) product compared to its precursor catalyst (commercial ZrO₂), which is found to be inactive catalyst for DEE from ethanol dehydration, even though it gives liquid yield. The catalytic selectivity of the SO₄/ZrO₂ samples is correlated well with increasing the amount of Brønsted and Lewis surface acid sites. The highest DEE content obtained was 1.62% using a ZS-1.5-500 catalyst at a reaction temperature of 225 °C.

Acknowledgements

The authors would like to acknowledge the financial support from Universitas Gadjah Mada under REKOGNISI TUGAS AKHIR (RTA) 2020 Program (Project number 2488/UN1.P.III/DIT-LIT/PT/2020).

References

- [1] B. Tabah, I.N. Pulidindi, V.R. Chitturi, L.M.R. Arava, A. Varvak, E. Foran, A. Gedanken, J. Mater. Chem. A. 5 (2017) 15486–15506.
- [2] Q. Ma, Q. Zhang, Z. Zheng, Fuel 288 (2021) 119832–119840.

- [3] J. Cho, W. Si, W. Jang, D. Jin, C.L. Myung, S. Park, *Appl. Energy* 160 (2015) 592–602.
- [4] H. Gürbüz, *Environ. Prog. Sustain Energy* 41 (2022) 13718–13727.
- [5] H.Y. Kim, J.C. Ge, N.J. Choi, *Appl. Sci.* 10 (2020) 1–15.
- [6] N. Kosaric, Z. Duvnjak, A. Farkas, H. Sahm, S. Bringer-Meyer, O. Goebel, D. Mayer, *Ethanol*, Wiley-Ullmann's Encyclopedia of Industrial Chemistry, New York, 2011.
- [7] R. Alviany, A. Wahyudi, I. Gunardi, A. Roesyadi, F. Kurniawansyah, D.H. Prajitno, *MATEC Web. Conf.* 156 (2018) 1–8.
- [8] I. Sezer, *Energy Environ.* 31 (2020) 179–214.
- [9] E. Chaichana, N. Boonsinvarothai, N. Chitpong, B. Jongsomjit, *J. Porous Mater.* 26 (2019) 599–610.
- [10] D.T. Sarve, S.K. Singh, J.D. Ekhe, *React. Kinet. Mech. Catal.* 131 (2020) 261–281.
- [11] C. Autthanit and B. Jongsomjit, *J. Oleo Sci.* 67 (2018) 235–243.
- [12] C. Krutpijit, B. Jongsomjit, *J. Oleo Sci.* 65 (2016) 347–355.
- [13] M. Limlamthong, N. Chitpong, B. Jongsomjit, *Bull. Chem. React. Eng. Catal.* 14 (2019) 1–8.
- [14] G. Garbarino, R.P.P. Vijayakumar, P. Riani, E. Finocchio, G. Busca, *Appl. Catal. B Environ.* 236 (2018) 490–500.
- [15] K. Wijaya, A.R. Putri, S. Sudiono, S. Mulijani, A. Patah, A.C. Wibowo, W.D. Saputri, *Catalysts* 11 (2021) 1492–1504.
- [16] K. Wijaya, M.L.L. Malau, M. Utami, S. Mulijani, A. Patah, A.C. Wibowo, M. Chadrsekaran, J.R. Rajabathar, H.A. Al-Lohedan, *Catalysts* 11 (2021) 1511–1523.
- [17] A.A. Frago-Mores de Oca, J.G. Hernández-Cortez, C. Angeles-Chaves, J.S. Valente, J.A. Toledo-Antonio, *Mater. Chem. Phys.* 291 (2022) 126659–126707.
- [18] I.S. Pieta, A. Michalik, E. Kraveva, D. Mrdenovic, A. Sek, E. Wahaczyk, A. Lewalska-Graczyk, M. Krysa, A. Sroka-Bartnicka, P. Pieta, R. Nowakowski, A. Lew, E. M. Serwicka, *Catalysts* 11 (2021) 660–680.
- [19] W. Alharbi, E. Brown, E.F. Kozhevnikova, I.V. Kozhevnikov, *J. Catal.* 319 (2014) 174–181.
- [20] M.F. Hanafi, N. Sapawe, *Mater. Today Proc.* 19 (2019) 1533–1536.
- [21] E. Dahdah, J. Estephane, C. Gennequin, A. Aboukais, E. Abi-Aad, S. Aouad, *Int. J. Hydrogen Energy* 45 (2020) 4457–4467.
- [22] A.R. Puigdollers, F. Illas, G. Pacchioni, *J. Phys. Chem. C* 120 (2016) 4392–4402.
- [23] L. Hauli, K. Wijaya, R. Armunanto, *Orient. J. Chem.* 34 (2018) 1559–1564.
- [24] F. Maleki, G. Pacchioni, *Top. Catal.* 63 (2020) 1717–1730.
- [25] Y. Zhou, W. Yang, X. Wang, S. Wang, Y. Wang, L. Zhang, J. Zhang, S. Tao, *Ind. Eng. Chem. Res.* 59 (2020) 21592–21601.
- [26] E. Hong, H.I. Sim, C.H. Shin, *Chem. Eng. J.* 292 (2016) 156–162.
- [27] K. Saravanan, B. Tyagi, H.C. Bajaj, *Appl. Catal. B Environ.* 192 (2016) 161–170.
- [28] Z. Mossayebi, M.J. Parnian, S. Rowshanzamir, *Macromol. Mater. Eng.* 303 (2018) 1–12.
- [29] X. Zhang, A.I.M. Rabee, M. Isaacs, A.F. Lee, K. Wilson, *ACS Sustain. Chem. Eng.* 6 (2018) 14704–14712.
- [30] Y. Qu, Y. Zhao, S. Xiong, C. Wang, S. Wang, L. Zhu, L. Ma, *Energy Fuels* 34 (2020) 11041–11049.
- [31] S. Yu, S. Wu, L. Li, X. Ge, *Fuel* 276 (2020) 118019–118024.
- [32] A.K. Amin, W. Trisunaryanti, K. Wijaya, *J. Nano Res.* 57 (2019) 31–39.
- [33] G. Shi, F. Yu, Y. Wang, D. Pan, H. Wang, R. Li, *Renew. Energy* 92 (2016) 22–29.
- [34] A. Kumar, S. Singhal, S. Agarwal, R.P. Badoni, A.R. Tripathi, *Int. J. Chem. Tech. Res.* 10 (2017) 350–358.
- [35] A.E.A.A. Said, M.A. El-Aal, *J. Fuel Chem. Technol.* 46 (2018) 67–74.
- [36] M. Utami, W. Trisunaryanti, K. Shida, M. Tsushida, H. Kawakita, K. Ohto, K. Wijaya, M. Tominaga, *RSC Adv.* 9 (2019) 41392–41401.
- [37] M. Ejtemaei, A. Tavakoli, N. Charchi, B. Bayati, A.A. Babaluo, Y. Bayat, *Adv. Powder Technol.* 25 (2014) 840–846.
- [38] A.K. Shah, M. Kumar, S.H.R. Abdi, R.I. Kureshy, N.H. Khan, H.C. Bajaj, *Appl. Catal. A Gen.* 486 (2014) 105–114.
- [39] M. Pérez, H. Armendáriz, J.A. Toledo, A. Vázquez, J. Navarrette, A. Montoya, A. García, *J. Mol. Catal. A Chem.* 149 (1999) 169–178.
- [40] M.S.L. Ore, K. Wijaya, W. Trisunaryanti, W.D. Saputri, E. Herald, N.W. Yuwana, P.L. Hariani, A. Budiman, S. Sudiono, *J. Environ. Chem. Eng.* 8 (2020) 104205–104214.
- [41] A. Patel, V. Brahmkhatri, N. Singh, *Renew. Energy* 51 (2013) 227–233.
- [42] A.E.A.A. Said, M.M.A. El-Wahab, M.A. El-Aal, *J. Mol. Catal. A Chem.* 394 (2014) 40–47.

- [43] D. Spielbauer, G.A.H. Mekhemer, M.I. Zaki, H. Knözinger, *Catal. Letters* 40 (1996) 71–79.
- [44] I.T.A. Aziz, W.D. Saputri, W. Trisunaryanti, S. Sudiono, A. Syoufian, A. Budiman, K. Wijaya, *Period. Polytech. Chem. Eng.* 66 (2022) 101–113.
- [45] A.I. Ahmed, S.A.El-Hakam, S.E. Samra, A.A. El-Khouly, A.S. Khder, *Colloids Surf. A: Physicochem. Eng. Asp.* 317 (2008) 62–70.
- [46] F. Heshmatpour, R.B. Aghakhanpour, *Adv. Powder Technol.* 23 (2012) 80–87.
- [47] V.S. Marakatti, S. Marappa, E.M. Gaigneaux, *New J. Chem.* 43 (2019) 7733–7742.
- [48] H. Yuan, Z. Dong, J. He, Y. Wang, H. Zhang, *Chem. Eng. Commun.* 206 (2019) 1618–1627.
- [49] T. Kamsuwan, P. Praserttham, B. Jongsomjit, *J. Oleo Sci.* 66 (2017) 199–207.
- [50] M.J. Marbun, F. Kurniawansyah, D.H. Prajitno, A. Roesyadi, *IOP Conf. Ser. Mater. Sci. Eng.* 543 (2019) 012058–012063.